Multifunctional Janus Microplates Arrays Actuated by Magnetic Fields for Water/Light Switches and Bio-Inspired Assimilatory Coloration

Shaojun Jiang, Yanlei Hu,* Hao Wu, Yachao Zhang, Yiyuan Zhang, Yulong Wang, Yinghui Zhang, Wulin Zhu, Jiawen Li, Dong Wu,* and Jiaru Chu

Smart dynamic regulation structured surfaces, inspired by nature, which can dynamically change their surface topographies under external stimuli for convertible fluidic and optical properties, have recently motivated significant interest for scientific research and industrial applications. However, there is still high demand for the development of multifunctional dynamically transformable surfaces using facile preparation strategies. In this work, a type of Janus high-aspect-ratio magnetically responsive microplates array (HAR-MMA) is readily fabricated by integrating a flexible laser scanning strategy, smart shape-memory-polymer-based soft transfer, and a simple surface treatment. By applying external magnetic field, instantaneous and reversible deformation of Janus HAR-MMA can be actuated, so surface wettability can be reversibly switched between superhydrophobic (158°) and hydrophilic (40°) states, based on which a novel magnetically responsive water droplet switch can be realized. Moreover, inspired by the biological assimilatory coloration of chameleons, dynamically color conversion can be skillfully realized by applying different colors on each side of the Janus HAR-MMA. Finally, as a proof-of-concept demonstration in light manipulation, a HAR-MMA is applied as an optical shutter actuated by external magnetic field with eximious controllability and repeatability. The developed multifunctional HAR-MMA provides a versatile platform for microfluidic, biomedical, and optical applications.

Diverse natural organisms show the impressive ability to dynamically change their interfacial properties on demand to respond to the external environments effectively. Examples of these dynamic regulation include that mimosa closes the leaves under external stimuli,[1] honeybee dynamically alter the wettability of tongue to reduce the energy consumption,[2] and many other animals such as chameleons and cephalopods are capable of changing skin or body colors rapidly for camouflage

or communication.[3,4] Inspired by these stimuli-responsive organisms, a variety of smart dynamic regulation structured surfaces (DRSSs) have been designed and manufactured.[5–7] Unlike the static surfaces covered with micro- and nanostructure, DRSS can change their surface topographies and properties by mechanically responding to external stimuli, enabling the regulation of multiple functions such as wettability,[5,8,9] optical transmittance,[10,11] and adhesion,[6,7,12] which are highly demanded both in academic researches and practical applications including microfluidic devices,[13,14] soft robotics,[15–18] and biomedical engineering.[19,20]

Till now, several different external stimuli have been explored to drive the DRSS such as mechanical forces,[8,21] pneumatics,[9] thermal,[7,22,23] or electric or magnetic fields.[24–30] Among them, magnetic actuation has the attractive advantages of high controllability, safe, noncontact features, and instantaneous response,[10,17,31] which are particularly promising for biomedical applications where remote actuation is typically required in a confined environment with uncontested safety. Soft elastomers have been applied as the magnetically responsive materials, on which multiple functions can be achieved by building different microstructures. Magnetically actuated microridges were constructed with outstanding dry adhesive ability to realize controllable capture and release of glass spheres.[6] Peng et al.[24] used the magnetically responsive conical arrays as the fog collector to capture static fog water under windless conditions. Surfaces with magnetically controllable micropillars were also applied to realize switchable topographies between superhydrophobic and slippery states,[5] transformation between water-repellent and water-adhesive states,[25] or directional microdroplet transporting.[32] Magnetically responsive hierarchical pillars were prepared on the polydimethylsiloxane (PDMS) substrate enables efficient manipulation of pure discrete droplet.[33] Directionally controlled anisotropic slippery surface was designed to realize unidirectional droplet adhesion and sliding by controlling the direction of ferromagnetic microcilia.[26] Ni wires arrays topped with hemispherical caps were

S. Jiang, Prof. Y. Hu, H. Wu, Y. Zhang, Y. Zhang, Y. Wang, Y. Zhang,
W. Zhu, Prof. J. Li, Prof. D. Wu, Prof. J. Chu
Hefei National Laboratory for Physical Sciences at the Microscale and
CAS Key Laboratory of Mechanical Behavior and Design of Materials
Department of Precision Machinery and Precision Instrumentation
University of Science and Technology of China
Hefei, Anhui 230027, China
E-mail: huyl@ustc.edu.cn; dongwu@ustc.edu.cn

**ADVANCED
SCIENCE NEWS**

www.advancedsciencenews.com

**ADVANCED
MATERIALS**

www.advmat.de

prepared by template-assisted electrodeposition approach, can be used for controlling their wetting properties remotely.[34] In addition to the aforementioned functions, magnetically responsive structures can be further used to transport nonmagnetic PS microspheres,[27] or transform between untethered 2D and 3D complex shapes.[15]

With the advance of sophisticated magnetic field control and mature fabrication techniques, recently the magnetically actuated surfaces have evolved from exhibiting a single function to possessing the ability of multiple functions.[28,31] Yet the facile integration of multiple functions in a structured surface still remains a grand challenge. Furthermore, the magnetically responsive surfaces developed so far involve relatively complicated multistep fabrications, which are either high cost, time consuming, or low throughput. Moreover, the performance of surface properties regulation depends mainly on the geometric characteristics and surface properties of the structure. The structures manufactured by the existing fabrication approaches are not scalable, resulting in limited regulation abilities. Therefore, it is highly desirable to manufacture novel multifunctional magnetically actuated surfaces with simplified structural morphology, convenient operation, and facile fabrication.

Herein, a low-cost prestretched shape-memory polystyrene (SMP) film is utilized as the template to prepare a brand-new magnetically actuated Janus microplates array on PDMS mixed with magnetic particles. As a kind of flexible micro/nanofabrication tool, femtosecond laser can realize one-step and maskless fabrication of structures with good scalability, which is difficult to achieve by either soft lithography or self-assembly. By combining the flexible femtosecond laser writing and the heating shrinkage property of SMP, the magnetic microplates array can be obtained with high aspect ratio. Subsequently, superhydrophobic spray treating, sunny-side-up laser scanning, and alternative color painting are employed to modify high-aspect-ratio magnetically-responsive microplates arrays (HAR-MMA) surface properties to launch the distinct multifunctionality of the Janus microplates array, including fast switchable wettabilities between superhydrophobic and hydrophilic states, selective water drop switch, adaptive surface colors transformation, and controllable light manipulation. The demonstrated multifunctional surfaces with Janus HAR-MMA unfold new capacities of DRSS in wider applications of liquid droplet manipulation, camouflage, and light-weight optical devices.
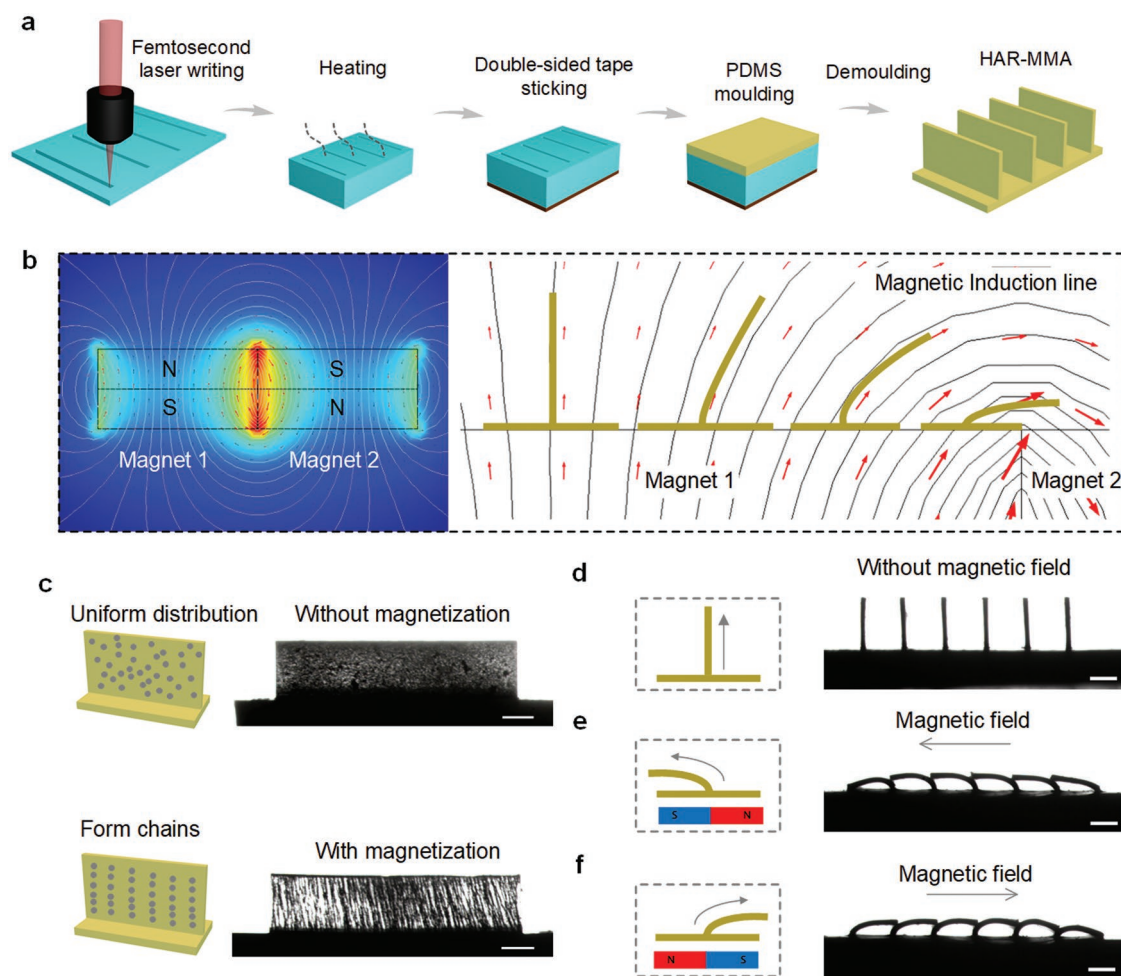
The fabrication process of HAR-MMA is schematically illustrated in **Figure 1**a. A series regular rectangular holes are constructed on the shape memory polystyrene polymer sheet through fast femtosecond laser writing strategy. Shape memory polymers (SMPs) are shape programmable materials that can be transformed from temporary shape to initial shape under external stimulation, and have been widely applied.[35,36] The polystyrene film has a relatively stable shrinkage ratio, so we can get a proportional relationship between the dimensions before and after shrinkage (Figure S1, Supporting Information). In order to obtain rectangular holes with higher aspect ratio, the polystyrene polymer sheet is heated in an oven at 130 °C for 9 min. After heated, the polystyrene film shrinks completely, the whole polystyrene sheet increases from original thickness ≈170 µm to final ≈960 µm in z-direction and retracts to ≈40% of its original size in x–y plane. So the initial laser writing

dimensions can be obtained according to the designed dimensions of the target SMP mold and the shrinkage ratio. The regular rectangular holes on the sheet change in the same way as the polystyrene polymer sheet, thus becoming narrower and deeper (Figure S2, Supporting Information), so the rectangular holes with higher aspect ratio are readily prepared. In order to make the rectangular holes become blind holes to prevent the PDMS from leaking, the double-sided tape is stuck to one side of the shrunk polystyrene sheet. Liquid PDMS mixed with carbonyl iron powder (3–5 µm particle size) in a weight ratio of 25% is then casted into the prepared polystyrene mold and degassed. To attain a strong magnetic response of external magnetic field and directional actuation, a neodymium–iron–boron (NdFeB) permanent magnet ($40 \times 40 \times 20$ mm) is placed below the sample for about 5 s to assemble the iron particles into chains. After cured in an oven (100 °C, 0.5 h), the double-sided tape is carefully peeled off so the polystyrene mold can be exposed. Then the polystyrene mold is dissolved in toluene solution under ultrasonic environment for 0.5 h. After that, the obtained HAR-MMA is further post-treated to eliminate the effect of toluene on the swelling of PDMS. The HAR-MMA is first treated in deionize water under ultrasonic environment for 10 min and then in ethanol for another 10 min. With the aid of post-treatment, there is no obvious swelling can be observed (Figure S3, Supporting Information).

The magnetic response property of the prepared HAR-MMA is examined by applying two jointed square NdFeB permanent magnets ($40 \times 40 \times 20$ mm, ≈0.34 T at the junction) at the bottom of the sample (Figure S4, Supporting Information). The magnetic field of two jointed magnets is simulated and the bending behavior of a microplate is analyzed. As shown in Figure 1b, microplate bends along the direction of the magnetic field, with the moving of magnets, microplate gradually bends as it approaches to the junction of two magnets, and finally reaches to the maximum bending degree at the junction. The bending is mainly caused by the magnetic torques within the carbonyl iron particles chains, which forces the microplate to align with the direction of the magnetic field.[17] As can be seen in Figure 1c, carbonyl iron particles uniformly distribute in the microplate without magnetization, and the microplate is hard to bend. After magnetization, chains are formed by the carbonyl iron particles along the magnetic field direction, and enhance the directional actuation (details can be seen in Figure S5, Supporting Information).

Figure 1d–f shows the side-view images of three different states of the HAR-MMA under actuation of magnetic fields with different directions. HAR-MMA bend along the direction of the magnetic field and recover to initial straight state without magnetic field. It is noteworthy that when the HAR-MMA bend on both sides, the top of the back microplate will lean against the root of the front microplate, thus forming a sealed continuous surface (Figure 1e,f, Video S1, Supporting Information), facilitating the following functionalization.

Figure 2a,b shows the scanning electron microscopy (SEM) images of the shape-memory polystyrene film sheet before and after shrinkage. The initial rectangular holes are fabricated on the SMP sheet with width of 260 µm, length of 5 mm, and the interval of 2 mm between two adjacent rectangular holes. After shrinkage, the width of the holes retracts to ≈110 µm and the

**ADVANCED
SCIENCE NEWS**
www.advancedsciencenews.com

**ADVANCED
MATERIALS**
www.advmat.de

Figure 1. Fabrication of the HAR-MMA and the magnetic-driven bending behaviors. a) Schematic illustration of fabrication procedure of HAR-MMA. b) Simulation of magnetic field and microplate bends into alignment with the magnetic field. c) Optical images of microplates without magnetization and with magnetization. Carbonyl iron particles uniformly distribute in the microplate without magnetization. Before curing, the sample is placed on the NdFeB permanent magnet for 5 s, so the carbonyl iron particles form into chains along the magnetic field direction. Left column shows the corresponding schematics. d–f) HAR-MMA bend under different magnetic field directions. Optical images show HAR-MMA keeping d) straight state without magnetic, and e,f) bending and forming an end-to-end continuous surface under magnetic field. Left columns of d–f) show the corresponding schematics. All scale bars: 500 μm.

length retracts to ≈2.1 mm, the interval reduced to ≈803 μm, and the contraction rate is ≈60%, consistent with that of bulk SMP without microstructures. The aspect ratio is changed from the original ≈0.65 to the final ≈8.73. By demolding from the above-mentioned mold, HAR-MMA with height of ≈940 μm, width (W) of ≈100 μm, length (L) of ≈2.1 mm, interval of ≈803 μm can be acquired as shown in Figure 2c,d. Based on this facile femtosecond laser processing technology and heating shrinkage property of SMP, HAR-MMA with different parameters can be obtained. As an example, another HAR-MMA with height of ≈930 μm, width of ≈140 μm, length of ≈4.5 mm, and interval of ≈805 μm is shown in Figure 2e,f, validating the flexibility and scalability of our fabrication method (more complex structures are shown in Figure S6, Supporting Information).

The bending properties of HAR-MMA with different parameters are systematically characterized by controlling the vertical distance between microplates array and magnets (dependence of magnetic flux density on distance is discussed in Figure S7, Supporting Information). We first fabricate several HAR-MMA with fixed width (104 μm) and different lengths, then varying the magnetic field by controlling the vertical distance of magnets and HAR-MMA. As can be seen in Figure 2g, the bending angle (θ, the site we measure the bending angle is shown in Figure 2h inset) decreases from 83.6° ± 4.2° to 30.5° ± 2.3° with the increase of magnetic flux density from 0 to 300 mT. With the same magnetic flux density, there is no obvious difference (less than 5° in the range of 100–300 mT) in the bending angle between HAR-MMA with different lengths. When the magnetic flux density is smaller than 100 mT, the bending angle is affected by the initial state (no magnetic field state) of microplates, and the slight deflection caused by magnetic torques is even smaller than the initial bending angle of the microplate. So with the same magnetic flux density, the difference of bending angle ranges from 9.5–17.3°. Bending angle versus magnetic field for HAR-MMA with different widths and fixed length of 2 mm
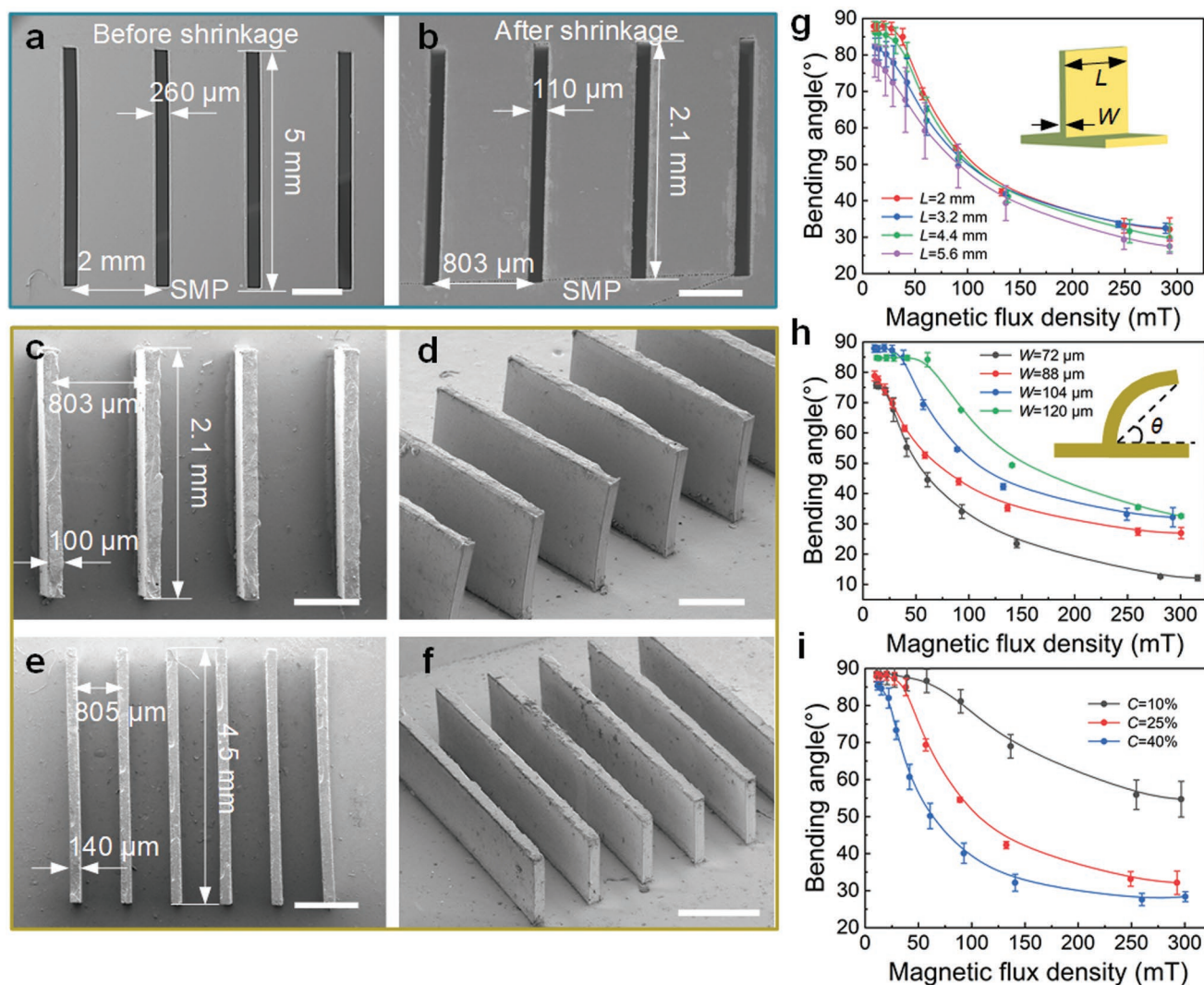
Figure 2. Dimension-controllable HAR-MMA and its magnetically responsive bending property. SEM images of SMP a) before shrinkage and b) after shrinkage. Scale bars are a) 1 mm and b) 500 µm, respectively. c–f) SEM images of HAR-MMA with different parameters. c,d) HAR-MMA with W of ≈100 µm, L of ≈2.1 mm, and interval of ≈803 µm, the height of microplate is ≈940 µm. e,f) HAR-MMA with W of ≈140 µm, L of ≈4.5 mm and interval of ≈805 µm, the height of microplate is ≈930 µm. Scale bars are c,d) 500 µm, and e,f) 1 mm, respectively. g) The quantitative relationship between bending angle and magnetic flux density of HAR-MMA with W of 104 µm, L of 2, 3.2, 4.4, and 5.6 mm, respectively. Inset is the schematic representation of W and L. h) The quantitative relationship between bending angle and magnetic flux density of HAR-MMA with L of 2 mm, W of 72, 88, 104, and 120 µm, respectively. Inset is the schematic representation of the bending angle. i) The quantitative relationship between bending angle and magnetic flux density of HAR-MMA with L of 2 mm, W of 104 µm, C of 10%, 25%, and 40%, respectively.

is shown in Figure 2h. Under the same magnetic flux density, bending angle increased with the increase of width (means that the bending degree decreased). The influence of carbonyl iron powder concentration (C) on the magnetically driven bending behavior is also investigated. Three HAR-MMA with different weight ratio of carbonyl iron powder to PDMS are constructed. The lengths and widths of the three microplates arrays are 2 mm and 104 µm, respectively. As we can see in Figure 2i, under the same magnetic flux density, the bending degree of HAR-MMA increases (θ decreased) as the concentration of iron powder increases. The angle ranged from 88.8° to 54.7°, 87.8° to 32.1°, and 85.3° to 28.4° corresponding to the carbonyl iron powder concentrations C = 10%, C = 25%, and C = 40%, respectively.

The magnetomechanical characteristics of HAR-MMA are modeled here. Due to the large deformation of HAR-MMA, a microplate can be considered as a rigid plate with an elastic torsion spring at its base.[6,28] The bending angle can be expressed by (elaborated in detail in the Supporting Information)

$$\theta = \frac{12 f_{\text{weight}} \rho_{\text{PDMS}} M B H^2}{\rho_m C_0 E W^2} \cos(\alpha + \theta) + \frac{\pi}{2}$$

where θ is the bending angle (Figure 2h inset), f_{weight} is the weight ratio of carbonyl iron powder to PDMS ($f_{\text{weight}} = C$), ρ_{PDMS} is the density of PDMS, M is the magnetization of the carbonyl iron particles, B is the magnetic flux density, H is the height of HAR-MMA, ρ_m is the density of carbonyl iron, C_0 is

the parametric angle coefficient, E is the elastic modulus of HAR-MMA (≈ 2.64 MPa, Figure S8, Supporting Information), W is the width of HAR-MMA, and α is the angle of the external magnetic field. From the equation we can see that the bending angle θ is inversely proportional to the weight ratio of carbonyl iron powder to PDMS (C) and proportional to the square of width of HAR-MMA. Furthermore, the bending angle has nothing to do with the length of HAR-MMA (L), showing good agreement between the experiments and the theoretical analysis (all the HAR-MMA is demolded from the SMP sheet with the same thickness, so H is constant here).

The bending direction of HAR-MMA can be reversibly switched by alternating the direction of the magnetic field. Unlike the previously developed DRSS with micropillars or microridges, the surface properties of HAR-MMA can be selectively modified. Under strong magnetic field gradient, microplates can be fully bent and form an end-to-end continuous surface, based on which Janus HAR-MMA can be manufactured. The fabrication process of Janus HAR-MMA is shown in **Figure 3**a. First a facile superhydrophobic spray method is used to modify the HAR-MMA to obtain excellent superhydrophobic property. After modification
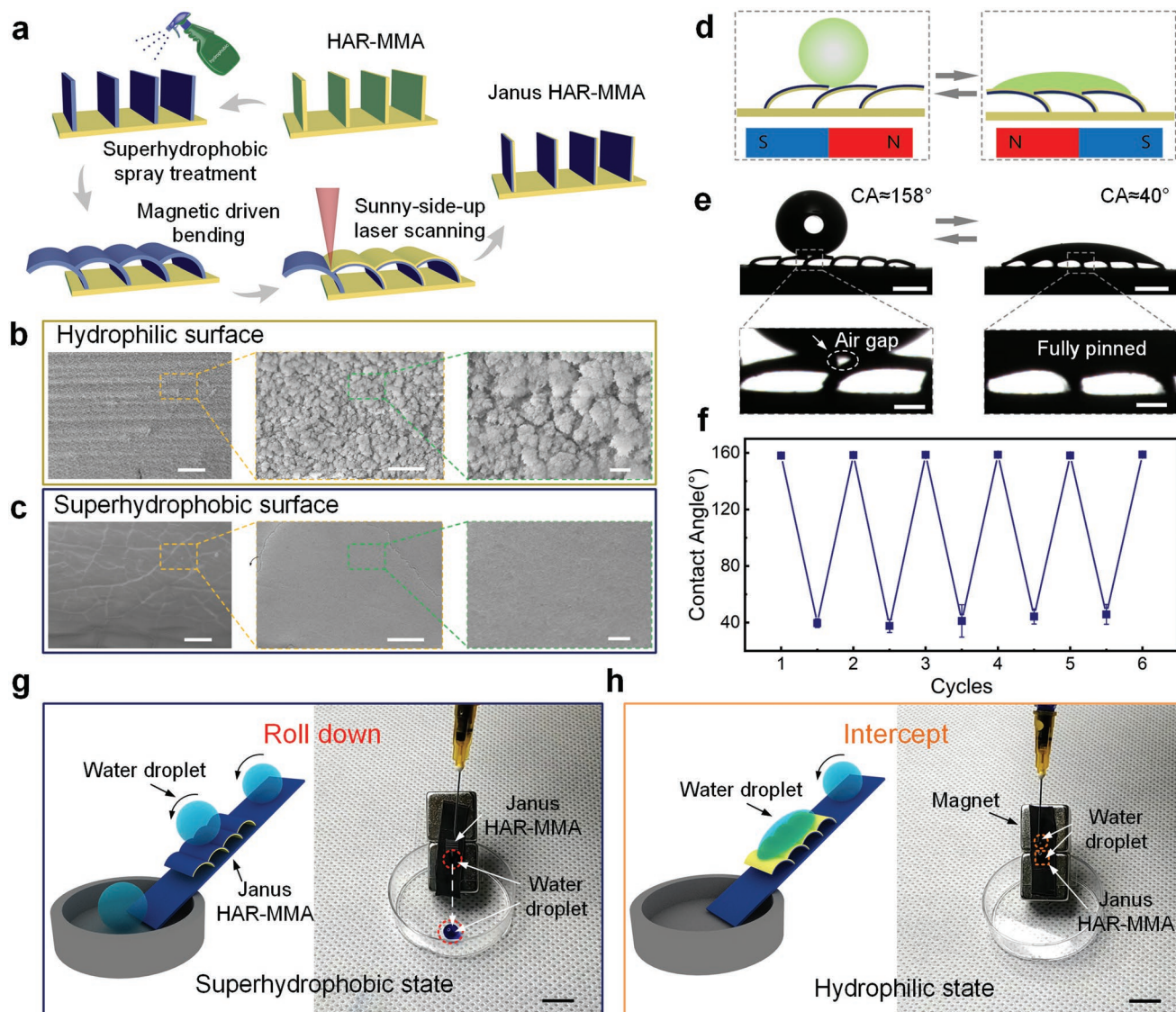
Figure 3. Switchable wettability of Janus HAR-MMA and magnetically responsive water droplet switch. a) Schematic illustration of the Janus HAR-MMA fabrication. b) SEM images of hydrophilic surface. It can be seen that the hydrophilic surface is covered by cauliflower-like micro-nanostructures. Scale bars are 50,10, and 2 μm respectively from left to right. c) SEM images of superhydrophobic surface. The surface is covered by a superhydrophobic material consisting of ≈40 nm nanoparticles. Scale bars are 50,10, and 2 μm respectively from left to right. d) Schematic of switchable wettability of Janus HAR-MMA. e) Optical images of a water drop on the superhydrophobic surface and hydrophilic surface. There is an air gap between water droplet and two microplates on the superhydrophobic surface, but water is fully pinned on the hydrophilic surface. Scale bars are 1 mm (upper), and 500 μm (lower), respectively. f) Reversible switching of water CAs, achieved by alternating the bending direction of HAR-MMA. g) Water droplet rolls down Janus HAR-MMA which is superhydrophobic state. Scale bar: 1 cm. h) Water droplet is intercepted by Janus HAR-MMA which is hydrophilic state. Scale bar: 1 cm. Left columns of g,h) show the corresponding schematics.

with a commercial superhydrophobic spray which contains silica nanoparticles (≈40 nm) and organic reagent,[37,38] the water contact angle (CA) of the structured surface can be increased from ≈118° to 158° (Figure S9, Supporting Information). Then, in order to obtain a hydrophilic surface in one side of the HAR-MMA, a sunny-side-up laser scanning strategy is developed. The HAR-MMA is bent by putting magnets at the bottom, then the top plane is scanned by using femtosecond laser at a speed of 25 mm s⁻¹, a scanning space of 15 µm under the laser power of 250 mW. The superhydrophobic material is removed and the hydrophilic carbonyl iron particles are exposed after being scanned by laser (Figure S10, Supporting Information). In this way, the surface becomes hydrophilic because of the exposure of hydrophilic carbonyl iron particles. As shown in Figure 3b, the laser-treated side becomes rough and is covered by cauliflower-like micro-/nanostructures with size of 2–7 µm, the rough structure further enhances the hydrophilic property. However, the untreated side is still covered by the superhydrophobic material (Figure 3c). The surface chemical compositions are further investigated by using X-ray photoelectron spectroscopy (XPS), as shown in Figure S11 in the Supporting Information. Using the as-prepared Janus HAR-MMA, the surface can be dynamically switched between superhydrophobic and hydrophilic states by alternating the direction of the magnetic field (Figure 3d). When the superhydrophobic sides are facing up, water droplet (4 µL) can form a sphere on the surface, the CA reaches ≈158°. It can be observed that an air gap exists between water droplet and two microplates, revealing superhydrophobic Cassie state. Therefore, water droplet can sit on the superhydrophobic surface stably rather than leaking to the hydrophilic side. Water droplet can easily roll off from the superhydrophobic surface due to the teeny adhesion. Conversely, when hydrophilic sides are facing up, water will be fully pinned into the gap between two microplates, and water CA can be ≈40° (Figure 3e, Video S2, Supporting Information). The performance of reversible switching between superhydrophobic and hydrophilic states is verified in cycle tests, showing eximious stability and repeatability of the proposed Janus HAR-MMA (Figure 3f).

On the basis of above reversibly switchable wettability of Janus HAR-MMA, a novel magnetically responsive water droplet switch can be fabricated, based on which water can selectively roll down or be intercepted. As can be seen in Figure 3g, by putting on the two jointed magnets (15 × 15 × 10 mm), the superhydrophobic sides are facing up, Janus HAR-MMA show superhydrophobic state with teeny adhesion, so water droplets can easily roll down. However, when the hydrophilic sides are facing up, water droplets will be intercepted by the Janus HAR-MMA. Water droplets (≈28.4 µL) are firmly attached to the hydrophilic sides even the tilt angle of Janus HAR-MMA is ≈41.5°, which shows excellent interception performance. (The height, width, and length of Janus HAR-MMA are ≈939 µm, 114 µm, and 3.90 mm, respectively, with the total area ≈15.6 mm²; Figure 3h, Video S3, Supporting Information).

Many animals in nature such as cuttlefish and chameleon have evolved a promising ability to change their body or skin colors under different environments to camouflage themselves (**Figure** 4a). Inspired by these biological assimilatory coloration behaviors, we elaborately utilize magnetic field driven Janus HAR-MMA to switch colors of an identical sample surface, and realize the controllable dynamically color conversion. (The height, width, and length of HAR-MMA are ≈943 µm, 110 µm, and 3.76 mm, respectively, with the total area ≈15.04 mm².) We apply different colors (red and green) on each side of the microplates, and then control the bending direction of the Janus HAR-MMA by changing the direction of magnetic field (two jointed magnets, 15 × 15 × 10 mm). Schematic of color conversion is shown in Figure 4b. When the Janus HAR-MMA bend in different directions, the surface color can be dynamically switched, in this way the color of the Janus HAR-MMA can be consistent with the background color, just like chameleon hides itself on the branch (Figure 4c, Video S4, Supporting Information). Furthermore, dynamic conversion of multiple colors can be achieved through skilled structural design and more dimensional control of the magnetic field, showing broad potential applications.

Venetian blind is widely used in our daily life to control the light transmittance, which is operated by controlling the tilting angle of the slats. Similarly, the bending angle of HAR-MMA can be controlled (from ≈90° to the minimum angle) by the movement of magnets, acting like a venetian blind. Based on this mechanism, we develop a magnetically responsive optical shutter. HAR-MMA doped with carbonyl iron powder can block visible light due to ultralow transmittance. To make sure good optical transparency of the substrate, HAR-MMA with 40% weight ratio of carbonyl iron powder is prepared on PDMS with high transmittance (the height, width, and length of HAR-MMA are ≈935 µm, 117 µm, and 5.34 mm, respectively, with the total area ≈29.37 mm²). A laser pointer (532 nm wavelength) is used to as the light source (Figure 4d). When microplates keep perpendicular to the substrate without external magnetic field, light can pass through the interstices of the microplates, giving an overall laser power ≈5 mW, corresponding to the "light on" state (see Figure 4e). As the magnets move toward the sample, the magnetic flux density gradually increases, so the bending degree of HAR-MMA increases and some of the laser is shielded by the microplates and eventually drops to the lowest value (≈0 mW) at the largest bending degree, so the light is OFF (see Figure 4f). With the cyclically moving of magnets, HAR-MMA can reversibly switch between ON and OFF states. We verify the transmittance of laser in several cycles, and find that the HAR-MMA can be well manipulated to control the light transmittance, exhibiting eximious controllability and repeatability (Figure 4g, Video S5, Supporting Information). It should be mentioned that dynamically light manipulation is achieved here by simply moving the magnets, so the switch speed is determined by the movement speed of magnets. The switch speed is anticipated to be further improved to achieve excellent dynamic performance by applying fast magnet motion stages or electromagnetic coil.

In conclusion, HAR-MMA are fabricated flexibly based on facile femtosecond laser scanning strategy and smart SMP based soft transfer. Janus HAR-MMA with multiple novel functions such as robust switchable wettability, selective water drop switch, dynamically color conversion, and controllable light manipulation can be achieved with simple modifications. Compared with the state-of-art methods, femtosecond laser processing
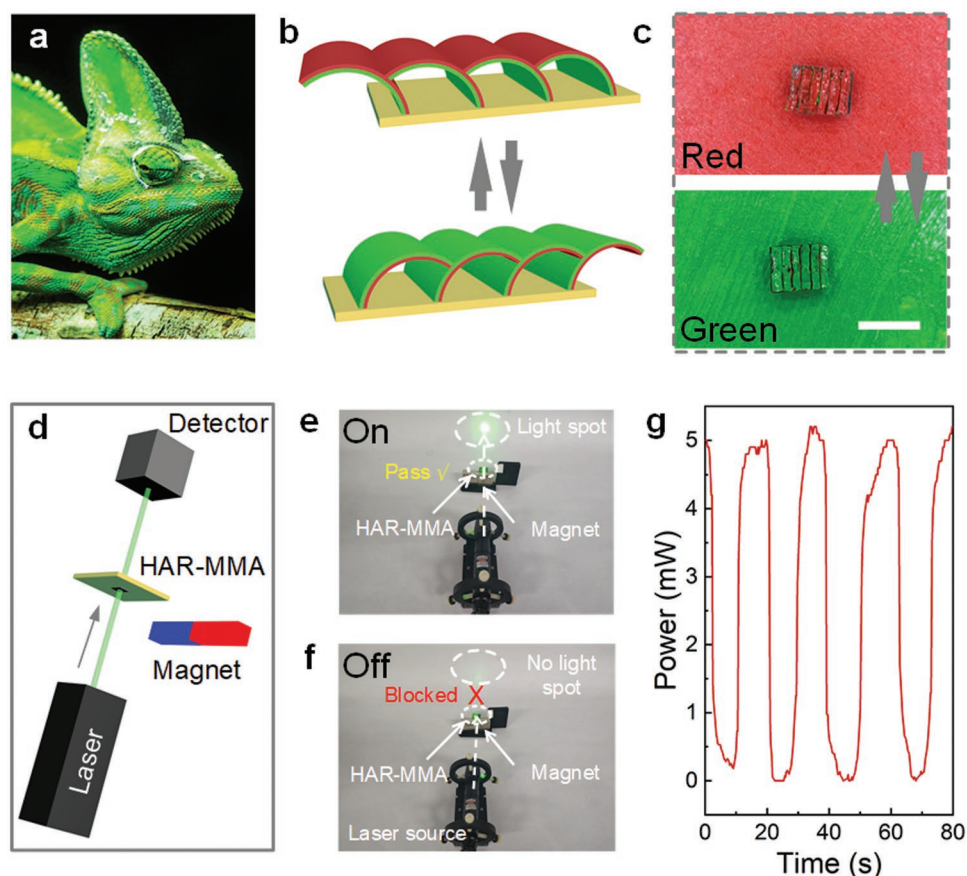
Figure 4. Dynamic color conversion and light manipulation. a) Photo of a chameleon, which is well known for its biological assimilatory coloration ability. b) Schematic of color conversion. The color of Janus HAR-MMA can be switched between red and green by simply magnetic responsive changing of the HAR-MMA orientation. c) Photos of Janus HAR-MMA switching between red and green. Scale bar: 5 mm. d) Schematic of magnetically driven optical shutter. Light on/off states can be switched by controlling the bending state of the HAR-MMA. e) Photo of optical shutter with light passing through the HAR-MMA. f) Photo of optical shutter with light blocked by the bended HAR-MMA. g) Continuous ON–OFF control of laser.

technology is a faster and more flexible strategy with the advantages of one-step and maskless fabrication of structures from micron to centimeter scales. Janus HAR-MMA are readily fabricated, and surface wettability can be reversibly switched from superhydrophobic to hydrophilic states by changing the bending direction of the HAR-MMA through simple magnetic field control strategy, based on which a novel magnetically responsive water droplet switch is developed for selective roll-down/interception of water droplets. Additionally, inspired by biological assimilatory coloration, magnetic-driven HAR-MMA suggest potential applications in dynamically color conversion. Finally, HAR-MMA can be used to dynamically alter the light transmittance by controlling the bending angle of microplates. Both the proposed facile fabrication method and the diverse paradigms of the as-prepared multifunctional DRSSs hold great promise in the applications of controllable surface wettability, microelectromechanical devices, optical communication, and manipulation.

Experimental Section

Materials: SMP was purchased from Hebei Bean Pod Network Technology Co., Ltd. The carbonyl iron powder was purchased from

Nangong Rui Teng Alloy Material Co., Ltd, with diameter of 3–5 μm (≥99.5% purity). Liquid polydimethylsiloxane (Sylgard 184, Dow Corning) was first mixed with carbonyl iron powder in a weight ratio of 25%, after thoroughly mixed, the cross-linker was added at a ratio of 10:1 (w/w) and thoroughly mixed again. Before PDMS molding, double-sided tape (Kapton, TED PELLA Inc., USA) was carefully stuck to one side of the shrunk SMP sheet. The magnets used in the experiment were purchased from Shanghai Ze He Mechanical & electrical co., Ltd. (40 × 40 × 20 mm) and Lanxi Ou Cheng Magnetic Industry Co., Ltd. (15 × 15 × 10 mm). The toluene (C_7H_8, ≥99.5% purity, 0.865 g cm^{-3} density) was used to dissolve the polystyrene mold. Ethanol (C_2H_6O >99.7% purity, 0.798 g cm^{-3} density) was used to post-treat the HAR-MMA. The superhydrophobic spray (Glaco Mirror Coat Zero, Soft 99 Ltd, Japan) was used to treat HAR-MMA, which contains silica nanoparticles (≈40 nm) and organic reagent.

Femtosecond Laser Fabrication: The laser beam (<100 fs, 1 kHz, 800 nm) from a Ti:sapphire femtosecond laser system (80L8TICE-ACE-100F-1K, Spectra-Physics Solstice Ace, USA) was employed to construct regular rectangular holes on the SMP sheet. Laser was focused on the SMP surface by a f-theta lens (focal length ≈100 mm), and the preprogramed rectangular scanning path was guided by a galvo-scanner system (s-9210d, Sunny Technology, China). By controlling the laser power at 250 mW, scanning speed at 25 mm s^{-1}, and scanning repetition of 50 circles, regular rectangular holes can be constructed on the SMP sheet.

Characterization: The topographies of SMP and HAR-MMA were characterized by using a secondary electron SEM (ZEISS EVO18). XPS

ADVANCED
SCIENCE NEWS

www.advancedsciencenews.com

ADVANCED
MATERIALS

www.advmat.de

(Thermo ESCALAB 250Xi) and field-emission transmission electron microscopy energy dispersive X ray analysis (JEM 2100F, JEOL, Japan) were used to characterize different surfaces of Janus microplate. XPS was conducted using a monochromatic Al-Kα X-ray source ($h\nu$ = 1486.6 eV). A CA100C contact-angle system (Innuo, China) was used to measure the water CAs ($\approx$4 µL water). The optical images were taken by a charge-coupled device camera and the carbonyl iron particles inside the microplate were observed by optical microscope (LW200-3JT). Magnetic flux density is measured with a digital Gauss meter (HM-100, Huaming instrument Co., Ltd., China). The magnetic field simulation result was obtained by using COMSOL software.

Supporting Information

Supporting Information is available from the Wiley Online Library or from the author.

Conflict of Interest

The authors declare no conflict of interest.

Keywords

dynamic regulation, femtosecond laser, magnetically responsive structure, multifunctional

[1] A. G. Volkov, J. C. Foster, V. S. Markin, *Plant, Cell Environ.* **2010**, *33*, 163.
[2] J. Chen, J. Wu, S. Yan, *J. Insect Sci.* **2015**, *15*, 164.
[3] J. Teyssier, S. V. Saenko, D. van der Marel, M. C. Milinkovitch, *Nat. Commun.* **2015**, *6*, 6368.
[4] C. C. Chiao, C. Chubb, R. T. Hanlon, *J. Comp. Physiol., A* **2015**, *201*, 933.
[5] Y. Huang, B. B. Stogin, N. Sun, J. Wang, S. Yang, T. S. Wong, *Adv. Mater.* **2017**, *29*, 1604641.
[6] A. G. Gillies, J. Kwak, R. S. Fearing, *Adv. Funct. Mater.* **2013**, *23*, 3256.
[7] H. Lee, D. S. Um, Y. Lee, S. Lim, H. J. Kim, H. Ko, *Adv. Mater.* **2016**, *28*, 7457.
[8] J.-N. Wang, Y.-Q. Liu, Y.-L. Zhang, J. Feng, H. Wang, Y.-H. Yu, H.-B. Sun, *Adv. Funct. Mater.* **2018**, *28*, 1800625.
[9] J.-N. Wang, Y.-Q. Liu, Y.-L. Zhang, J. Feng, H.-B. Sun, *NPG Asia Mater* **2018**, *10*, e470.
[10] S. Liu, Y. Long, C. Liu, Z. Chen, K. Song, *Adv. Opt. Mater.* **2017**, *5*, 1601043.
[11] S. Zeng, D. Zhang, W. Huang, Z. Wang, S. G. Freire, X. Yu, A. T. Smith, E. Y. Huang, H. Nguon, L. Sun, *Nat. Commun.* **2016**, *7*, 11802.
[12] D. M. Drotlef, P. Blumler, A. del Campo, *Adv. Mater.* **2014**, *26*, 775.
[13] A. R. Shields, B. L. Fiser, B. A. Evans, M. R. Falvo, S. Washburn, R. Superfine, *Proc. Natl. Acad. Sci. U. S. A.* **2010**, *107*, 15670.
[14] F. Fahrni, M. W. Prins, L. J. van Ijzendoorn, *Lab Chip* **2009**, *9*, 3413.
[15] Y. Kim, H. Yuk, R. Zhao, S. A. Chester, X. Zhao, *Nature* **2018**, *558*, 274.
[16] W. Hu, G. Z. Lum, M. Mastrangeli, M. Sitti, *Nature* **2018**, *554*, 81.
[17] M. M. Schmauch, S. R. Mishra, B. A. Evans, O. D. Velev, J. B. Tracy, *ACS Appl. Mater. Interfaces* **2017**, *9*, 11895.
[18] L. Hines, K. Petersen, G. Z. Lum, M. Sitti, *Adv. Mater.* **2017**, *29*, 1603483.
[19] S. Fusco, H. W. Huang, K. E. Peyer, C. Peters, M. Haberli, A. Ulbers, A. Spyrogianni, E. Pellicer, J. Sort, S. E. Pratsinis, B. J. Nelson, M. S. Sakar, S. Pane, *ACS Appl. Mater. Interfaces* **2015**, *7*, 6803.
[20] E. Gultepe, J. S. Randhawa, S. Kadam, S. Yamanaka, F. M. Selaru, E. J. Shin, A. N. Kalloo, D. H. Gracias, *Adv. Mater.* **2013**, *25*, 514.
[21] X. Yao, Y. Hu, A. Grinthal, T. S. Wong, L. Mahadevan, J. Aizenberg, *Nat. Mater.* **2013**, *12*, 529.
[22] S. Reddy, E. Arzt, A. del Campo, *Adv. Mater.* **2007**, *19*, 3833.
[23] J. Cui, D. M. Drotlef, I. Larraza, J. P. Fernandez-Blazquez, L. F. Boesel, C. Ohm, M. Mezger, R. Zentel, A. del Campo, *Adv. Mater.* **2012**, *24*, 4601.
[24] Y. Peng, Y. He, S. Yang, S. Ben, M. Cao, K. Li, K. Liu, L. Jiang, *Adv. Funct. Mater.* **2015**, *25*, 5967.
[25] C. Yang, L. Wu, G. Li, *ACS Appl. Mater. Interfaces* **2018**, *10*, 20150.
[26] M. Cao, X. Jin, Y. Peng, C. Yu, K. Li, K. Liu, L. Jiang, *Adv. Mater.* **2017**, *29*, 1606869.
[27] S. Ben, J. Tai, H. Ma, Y. Peng, Y. Zhang, D. Tian, K. Liu, L. Jiang, *Adv. Funct. Mater.* **2018**, *28*, 1706666.
[28] Z. Yang, J. K. Park, S. Kim, *Small* **2018**, *14*, 1702839.
[29] T. Deng, W. Zhang, O. Arcelus, J. G. Kim, J. Carrasco, S. J. Yoo, W. Zheng, J. Wang, H. Tian, H. Zhang, X. Cui, T. Rojo, *Nat. Commun.* **2017**, *8*, 15194.
[30] N. Verplanck, E. Galopin, J. C. Camart, V. Thomy, *Nano Lett.* **2007**, *7*, 813.
[31] Y. Zhu, D. S. Antao, R. Xiao, E. N. Wang, *Adv. Mater.* **2014**, *26*, 6442.
[32] Y. Lin, Z. Hu, M. Zhang, T. Xu, S. Feng, L. Jiang, Y. Zheng, *Adv. Funct. Mater.* **2018**, *28*, 1800163.
[33] J. H. Kim, S. M. Kang, B. J. Lee, H. Ko, W. G. Bae, K. Y. Suh, M. K. Kwak, H. E. Jeong, *Sci. Rep.* **2016**, *5*, 17843.
[34] A. Grigoryev, I. Tokarev, K. G. Kornev, I. Luzinov, S. Minko, *J. Am. Chem. Soc.* **2012**, *134*, 12916.
[35] R. Liu, X. Kuang, J. Deng, Y. C. Wang, A. C. Wang, W. Ding, Y. C. Lai, J. Chen, P. Wang, Z. Lin, H. J. Qi, B. Sun, Z. L. Wang, *Adv. Mater.* **2018**, *30*, 1705195.
[36] J. G. Hardy, M. Palma, S. J. Wind, M. J. Biggs, *Adv. Mater.* **2016**, *28*, 5717.
[37] A. Jetly, I. U. Vakarelski, S. T. Thoroddsen, *Soft Matter* **2018**, *14*, 1608.
[38] I. U. Vakarelski, N. A. Patankar, J. O. Marston, D. Y. Chan, S. T. Thoroddsen, *Nature* **2012**, *489*, 274.